Objective constitutive relations from DEM

Stefan Luding

Abstract: Powders in a split-bottom ring shear cell geometry show wide shear bands under slow, quasi-static deformation. From discrete element simulations (DEM), several continuum fields like the density, velocity, deformation gradient and stress are computed and evaluated with the goal to formulate objective constitutive relations for the powder flow behavior.

From a single simulation, by applying time- and local space-averaging, a nonlinear yield surface is obtained with a peculiar stress dependence. Stress and strain are observed to be not perfectly co-linear, and the difference in orientation seems to be decaying with shear-rate.

The anisotropy is always smaller than the macroscopic friction coefficient. However, the lower bound of anisotropy increases with the shear rate, approaching the maximum according to a stretched exponential with a specific rate that is consistent with a shear path of about one particle diameter.

1 Introduction

Powders or sand consist of many independent particles with peculiar collective flow behavior. Knowing the interaction laws and inserting those into a discrete element model (DEM), one can follow the particles by integrating Newtons equations of motion (Herrmann, Hovi, and Luding 1998; Kishino 2001; Luding, Lätzel, and Herrmann 2001; Luding 2004b; Luding 2008b).

The goal can be to derive continuum constitutive relations – as needed for industrial application. Methods and tools for a so-called micro-macro transition are applied (Vermeer, Diebels, Ehlers, Herrmann, Luding, and Ramm 2001; Lätzel, Luding, and Herrmann 2000; Luding 2004a; Luding 2005b; Luding 2005a) on small so-called representative volume elements (RVE). In the ring-shear cell, both local space averaging (on toroidal sub-volumes at fixed radial and vertical position) as well as time-averaging in the (presumed) steady state can be applied and one obtains already from a single simulation some of the constitutive relation aimed for.

In this study, the micro-macro averaging is applied to a three-dimensional split-bottom shear cell as recently presented (Fenistein and van Hecke 2003; Fenistein, van de Meent, and van Hecke 2004). The special property of a split-bottom ring shear cell is the fact that the shear band is initiated at the bottom slit and its velocity field is well approximated by an error-function

(Fenistein, van de Meent, and van Hecke 2004; Luding 2004b; Luding 2006b) with a width considerably increasing from bottom to top (free surface). In this study, the frictionless data are examined and the stress- and strain-tensors are examined in their eigensystems and eigendirections.

2 The Soft Particle Molecular Dynamics Method

The behavior of granular media can be simulated with the discrete element method (DEM) (Allen and Tildesley 1987; Lätzel, Luding, Herrmann, Howell, and Behringer 2003; Luding 2008a). The most basic ingredient is a force-displacement relation that governs the interaction between pairs of particles. Particle positions, velocities and interaction forces are then sufficient to integrate (explicitly) Newtons equations of motion and follow all particles during their evolution in time.

Since the realistic modeling of the deformations of the particles is much too complicated, we relate the normal interaction force to the overlap as $f = k\delta$, with a stiffness k, if $\delta > 0$. In order to account for energy dissipation, the normal degrees of freedom, i.e. the relative motion of two particles in contact, is subject to a viscous, velocity dependent damping, for more details see (Luding 1998; Luding 2006a; Luding 2008a).

3 Ring shear cell in 3D

In order to save computing time, only a quarter of the ring-shaped geometry is simulated. The walls are cylindrical, and are roughened due to some (about 3 per-cent of the total number) attached particles (Luding 2004b; Luding 2006b; Luding 2008b). The outer cylinder wall with radius $R_o = 0.110\,\mathrm{m}$, and part of the bottom $r > R_s = 0.085\,\mathrm{m}$ are rotating around the symmetry axis, while the inner wall with radius $R_i = 0.0147\,\mathrm{m}$, and the attached bottom-disk $r < R_s$ remain at rest. For small filling height, the shearband is visible from the top, whereas for larger filling height, the shearband does not reach the top and other modes of flow can be observed, see Ref. (Luding 2008b).

3.1 Material and system parameters

First, the simulation runs for more than 50 s with a rotation rate $f_o = 0.01\,\mathrm{s}^{-1}$ of the outer cylinder, with angular velocity $\Omega_o = 2\pi f_o$. For the average only larger times are taken into account, thus disregarding the transient behavior at the onset of shear. A snapshot in steady state (top and front view) is displayed in Fig. 1.

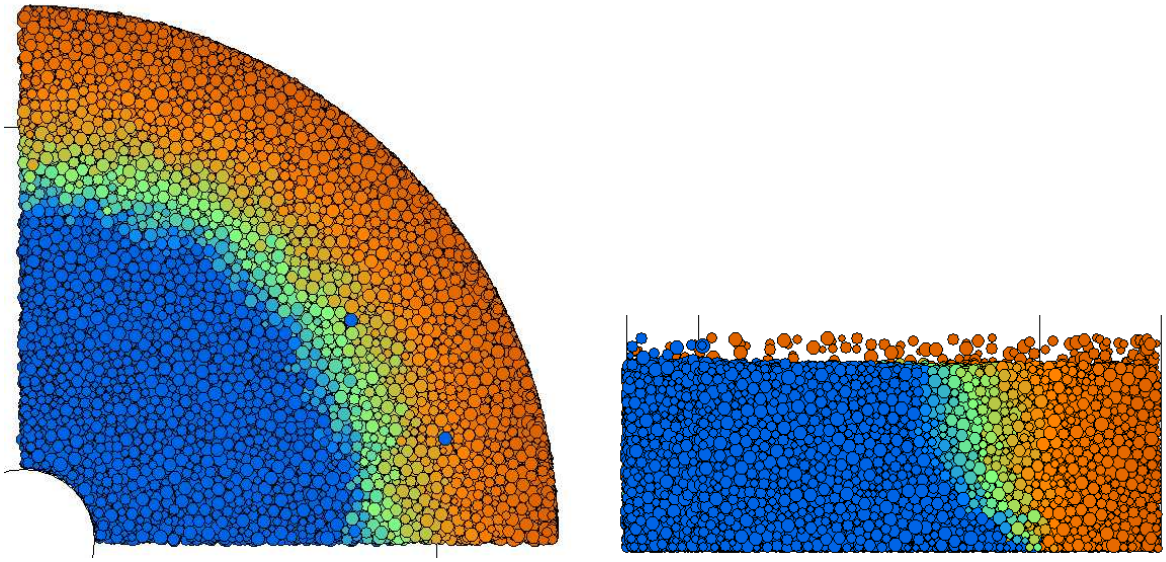

Figure 1: Snapshots from a simulation with $N = 34518$ particles, without friction $\mu = 0$. The colors blue, green, orange and red denote particles with displacements in tangential direction per second $r\,\mathrm{d}\phi \leq 0.5\,\mathrm{mm}$, $r\,\mathrm{d}\phi \leq 2\,\mathrm{mm}$, $r\,\mathrm{d}\phi \leq 4\,\mathrm{mm}$, and $r\,\mathrm{d}\phi > 4\,\mathrm{mm}$.

3.2 Averaging and micro-macro procedure

Since we assume translational invariance in the tangential ϕ-direction, averaging is performed over toroidal volumina and over many snapshots in time (typically 40-60), leading to fields $Q(r,z)$ as function of the radial and vertical positions. Here, averaging is performed with spacings of $\Delta r \approx 0.0025$ and $\Delta z \approx 0.0028$ in radial and vertical direction.

From the simulations, one observes that the density, the coordination number and the isotropic fabric decrease with height and are systematically lower in the shear band due to dilatancy. From a set of simulations with different filling heights (data not shown, see (Luding 2004b)), just examined from the top (like in the original experiments), it becomes clear that the shearband moves inwards with increasing filling height and also becomes wider. From the front-view, the same information can be evidenced, see Fig. 1, as well as the shape and width of the shear band inside the bulk. The shear band moves rapidly inwards deep in the bulk – close to the slit in the bottom – while its position does not change much more further up.

From the velocity field gradient, the strain rate

$$\dot\gamma = \sqrt{d_1^2 + d_2^2} = \frac{1}{2}\sqrt{\left(\frac{\partial v_\phi}{\partial r} - \frac{v_\phi}{r}\right)^2 + \left(\frac{\partial v_\phi}{\partial z}\right)^2}\,, \tag{1}$$

can be obtained, as discussed in Ref. (Depken, van Saarloos, and van Hecke 2006), see Eq. (7) therein (the geometrical term, v_ϕ/r in Eq. (1), comes from the cylindrical coordinate system used here). From the eigenvalue analysis of the velocity gradient, one finds that shear planes are well described by the normal unit vector $\hat\gamma = (\cos\theta, 0, \sin\theta)$, with $\theta = \theta(r,z) = \arccos(d_1/\dot\gamma)$, as predicted in Ref. (Depken, van Saarloos, and van Hecke 2006). This unit-vector, $\hat\gamma$, is the

eigen-vector of the vanishing eigenvalue of the velocity gradient tensor, while the other two are opposite-equal, with their eigen-vectors in the plane perpendicular to $\hat{\gamma}$.

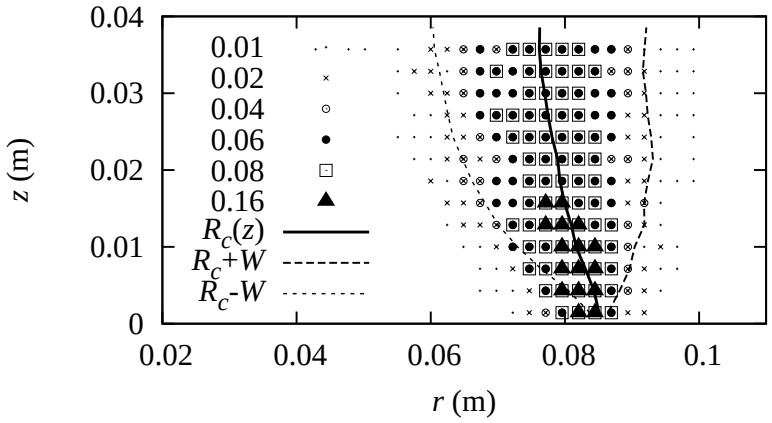

Figure 2: Graphic representation of the strain rate $\dot{\gamma}$, as given in the inset, plotted as function of radial and vertical positions – larger symbols correspond also to larger $\dot{\gamma}$. The lines indicate the center R_c and the half-width W of the shear band. (Luding 2008)

From the simulation, one can determine the components of the stress tensor

$$\sigma_{\alpha\beta} = \frac{1}{V} \sum_{c \in V} f_\alpha l_\beta \ , \tag{2}$$

with the components of the contact normal forces f_α and branch vectors l_β. The sum extends over all contacts within or close to the averaging volume, V, weighted according to their vicinity.

Since the $\sigma_{rz} \approx 0$ component is small, as compared to the other averaged non-diagonal stresses, the shear stress can be defined in analogy to the velocity gradient, as proposed in (Depken, van Saarloos, and van Hecke 2006):

$$|\tau| = \sqrt{\sigma_{r\phi}^2 + \sigma_{z\phi}^2} \ . \tag{3}$$

A more detailed study of the stress- and strain eigenvalues and eigensystems leads to the three eigenvalues $\sigma_{\max}$, σ_0, and $\sigma_{\min}$ corresponding to the maximum, intermediate and minimum stress, respectively, with corresponding eigen-directions $\hat{\sigma}_{\max}$, $\hat{\sigma}_0$, and $\hat{\sigma}_{\min}$. In Fig. 4, the shear stress $|\tau|$ and the deviator stress $\sigma_D = \sqrt{(\sigma_{\max} - \sigma_{\min})^2 + (\sigma_{\max} - \sigma_0)^2 + (\sigma_0 - \sigma_{\min})^2}/\sqrt{6}$ are plotted against the pressure $p = (\sigma_{\max} + \sigma_0 + \sigma_{\min})/3$. Note that the definition of σ_D is equivalent to $q = (\sigma_{\max} - \sigma_{\min})/2$ in the case of a stress tensor with $\sigma_0 = (\sigma_{\max} - \sigma_{\min})/2$.

Shear stress, τ, and deviator σ_D quantify the stress anisotropy and are almost identical, see Figs. 3 and 4, only σ_D appears systematically somewhat larger than $|\tau|$. The ratio $\sigma_D/\tau > 1$ is a decaying function of the shear rate (data not shown here – but note their big scatter) and indicates how good the stress tensor conforms with the assumptions that lead to Eq. (3). The closer the ratio is to unity, the closer the presumed stress is to the objective stress.

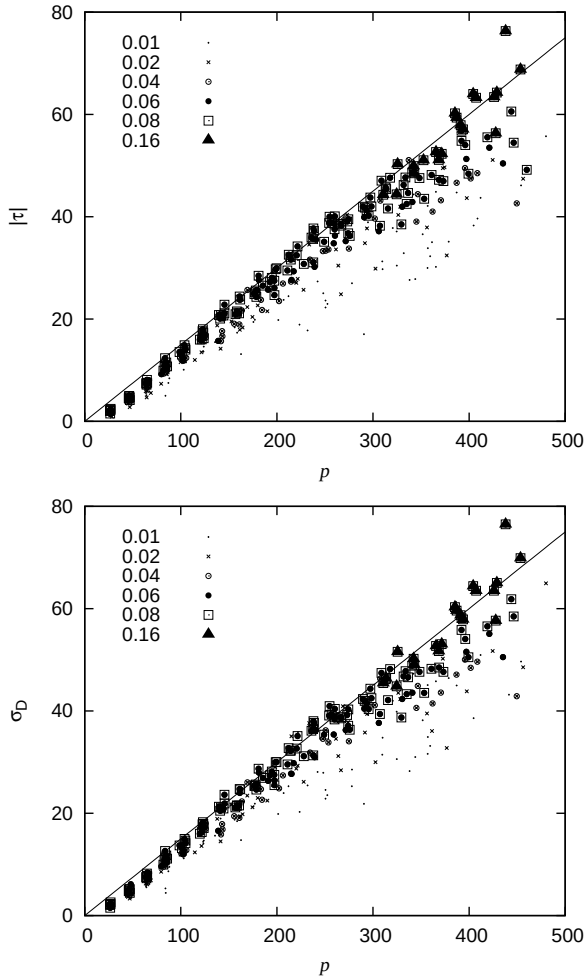

Figure 3: Shear stress $|\tau|$ and deviator stress σ_D, plotted against pressure p for different strain rates, limits are given in the inset. All points with higher shear rate are found close to the yield surface μp, as represented by the solid line, with constant $\mu = 0.15$.

From the (almost) constant shear stress intensity in the shear zone, one can determine the Mohr-Coulomb-type friction angle of the equivalent macroscopic constitutive law, as $\psi \approx \arcsin \mu$. Interestingly, without friction ψ is rather large, i.e., much larger than expected from a frictionless material, whereas it is astonishingly small with friction (data not shown, see (Luding 2008b)). From Fig. 4, one observes that the anisotropy is stress dependent, increasing up to moderate stress levels and then remaining more or less constant, within the fluctuations.

Plotting the shear stress intensity $|\tau|/p$ and the anisotropy σ_D/p against the shear rate $\dot{\gamma}$, or the non-dimensional shear rate

$$I = \dot{\gamma} d_0 \sqrt{\varrho/p}\,, \tag{4}$$

with the mean particle diameter d_0, and the bulk density, ϱ, as proposed in Ref. (MiDi 2004), neither leads to a better trend nor a better data collapse for either of the two possibilites. There-

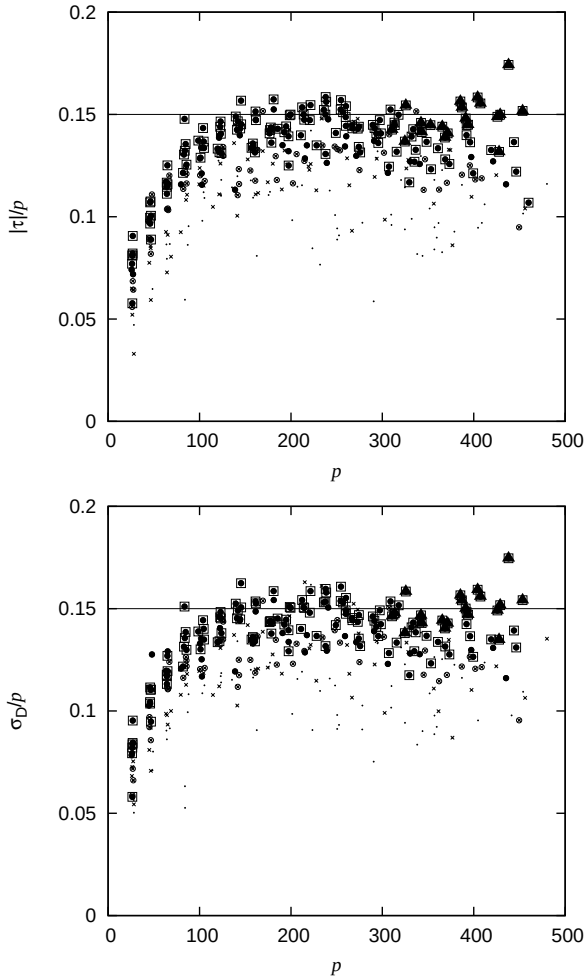

Figure 4: (Left) Shear stress ratio $|\tau|/p$ and (Right) anisotropy σ_D/p, plotted against pressure p for different strain rates as given in the inset.

fore, we define the dimensionless shear path

$$l_d = \frac{\Delta t\, \Delta r}{d_0}\, \dot{\gamma}\ , \tag{5}$$

with the simulation averaging time interval $\Delta t = 25.4\,\mathrm{s}$, and the radial bin-width, $\Delta r = 2.45\,10^{-3}\,\mathrm{m}$, used to compute the velocity gradient. The shear-path, l_d, indicates about how many particle diamters the shear planes have been sheared relative to each other.

When plotting $|\tau|/p$ and σ_D/p, in Fig. 5, against the shear path, l_d, the former appears (again) somewhat smaller than the latter. The question whether the very small systematic discrepancy between shear stress and deviator stress have a physical meaning or are only a consequence of statistical fluctuations can only be answered by a more careful analysis of the stress, the fabric, and the velocity gradient, which is far from the scope of this paper.

Besides considerable scatter, the data in Fig. 5 (Right) fall between the maximum anisotropy,

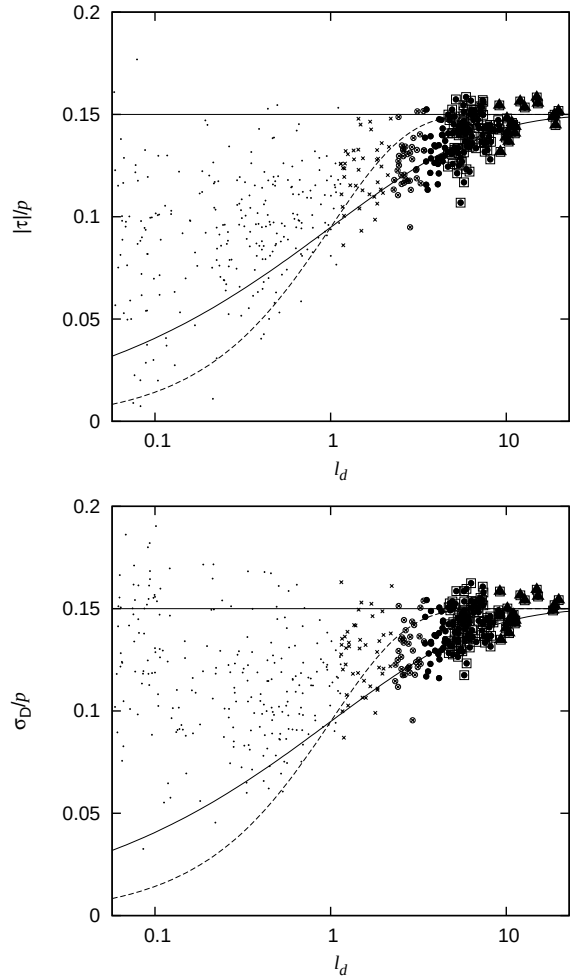

Figure 5: (Left) Shear stress intensity $|\tau|/p$, and (Right) anisotropy σ_D/p, plotted against the shear path l_d. The data for small pressures $p < 100$ are disregarded here. The solid and the dashed lines correspond to Eq. (6), with $\alpha = 0.5$ and $\alpha = 1$, respectively.

$\mu = 0.15$, and the lower bound:

$$\frac{\sigma_D}{p} > \mu \left[1 - \exp\left(-l_d^{\alpha}\right)\right] , \tag{6}$$

where the exponent $\alpha = 0.5$ seems to be a better choice than $\alpha = 1$. Note, however, that this is only an empirical fit-function without a theoretical basis. The stretched exponential lower bound indicates slow relaxation processes, which require that the granular material shear planes move relative to each other by much more than one particle diameter, before the steady state shear regime with anisotropy $\sigma_D/p \approx \mu$ is reached.

Thus anisotropy requires a certain shear path before its established and fully developed. This minimal displacement is consistent with the particle diameter, but a much more detailed parameter study is required to confirm this.

A local anisotropy, $s_D := \sigma_D/p$, starting from random initial situations, $0 \leq s_D \leq \mu$, and

evolving according to

$$\frac{\partial s_D}{\partial l_D} = (\mu - s_D) \ , \tag{7}$$

would be consistent with $\alpha = 1$, see the two-dimensional results (Luding 2004a). A quantitative confirmation of the above evolution law for the stress anisotropy with shear deformation is subject to further study of both steady and transient states.

4 Conclusion

Simulations of a slit-bottom Couette ring shear cell show perfect qualitative and good quantitative agreement with experiments. Frictionless simulations are already in 80% percent agreement with the experiments - and the simulation with friction comes even close to 90%. This is remarkable, since besides the geometry of the shear cell no special attention was payed to the choice of material parameters, particle-size and particle size distribution.

From the simulations, we learn that the shear-planes are tilted from the horizontal as proposed in Ref. (Depken, van Saarloos, and van Hecke 2006). The shear stress intensity is computed – under the assumption that the stress eigen-system is co-linear with the velocity gradient eigen-system – and compared to the objective stress anisotropy. The latter is always larger than the former, decreasing with shear rate to values close to unity.

The objective stress anisotropy is limited by the macroscopic friction coefficient $\mu \approx 0.15$. Shear planes with small shear rate occur with all values, $\mu \geq s_D \geq 0$, while the anisotropy is limited by a lower bound that approaches μ with increasing shear path. The major conclusion is that shear planes have to move relative to each other by more than one particle diameter before the maximum anisotropy can be established.

The functional behavior of the evolution of anisotropy with shear path has to be studied further for different parameters, system sizes, simulation duration, and also for transient states.

5 Acknowledgements

We acknowledge the financial support of several funding institutions that supported the reviewed research, the Deutsche Forschungsgemeinschaft (DFG), and the Stichting voor Fundamenteel Onderzoek der Materie (FOM), financially supported by the Nederlandse Organisatie voor Wetenschappelijk Onderzoek (NWO). Furthermore, helpful discussions with M. van Hecke and D. Wolf are acknowledged.

Literatur

Allen, M. P. and D. J. Tildesley (1987). *Computer Simulation of Liquids*. Oxford: Oxford University Press.

Depken, M., W. van Saarloos, and M. van Hecke (2006). Continuum approach to wide shear zones in quasistatic granular matter. *Phys. Rev. E 73*, 031302.

Fenistein, D., J. W. van de Meent, and M. van Hecke (2004). Universal and wide shear zones in granular bulk flow. *Phys. Rev. Lett. 92*, 094301. e-print cond-mat/0310409.

Fenistein, D. and M. van Hecke (2003). Kinematics – wide shear zones in granular bulk flow. *Nature 425*(6955), 256.

Herrmann, H. J., J.-P. Hovi, and S. Luding (Eds.) (1998). *Physics of dry granular media - NATO ASI Series E 350*, Dordrecht. Kluwer Academic Publishers.

Kishino, Y. (Ed.) (2001). *Powders & Grains 2001*, Rotterdam. Balkema.

Lätzel, M., S. Luding, and H. J. Herrmann (2000). Macroscopic material properties from quasi-static, microscopic simulations of a two-dimensional shear-cell. *Granular Matter 2*(3), 123–135. e-print cond-mat/0003180.

Lätzel, M., S. Luding, H. J. Herrmann, D. W. Howell, and R. P. Behringer (2003). Comparing simulation and experiment of a 2d granular couette shear device. *Eur. Phys. J. E 11*(4), 325–333.

Luding, S. (1998). Collisions & contacts between two particles. In H. J. Herrmann, J.-P. Hovi, and S. Luding (Eds.), *Physics of dry granular media - NATO ASI Series E350*, Dordrecht, pp. 285. Kluwer Academic Publishers.

Luding, S. (2004a). Micro-macro models for anisotropic granular media. In P. A. Vermeer, W. Ehlers, H. J. Herrmann, and E. Ramm (Eds.), *Modelling of Cohesive-Frictional Materials*, Leiden, Netherlands, pp. 195–206. Balkema. (ISBN 04 1536 023 4).

Luding, S. (2004b). Molecular dynamics simulations of granular materials. In H. Hinrichsen and D. E. Wolf (Eds.), *The Physics of Granular Media*, Weinheim, Germany, pp. 299–324. Wiley VCH.

Luding, S. (2005a). Anisotropy in cohesive, frictional granular media. *J. Phys.: Condens. Matter 17*, S2623–S2640.

Luding, S. (2005b). Shear flow modeling of cohesive and frictional fine powder. *Powder Technology 158*, 45–50.

Luding, S. (2006a). About contact force-laws for cohesive frictional materials in 2d and 3d. In P. Walzel, S. Linz, C. Krülle, and R. Grochowski (Eds.), *Behavior of Granular Media*, pp. 137–147. Shaker Verlag. Band 9, Schriftenreihe Mechanische Verfahrenstechnik, ISBN 3-8322-5524-9.

Luding, S. (2006b). Particulate solids modeling with discrete element methods. In P. Massaci, G. Bonifazi, and S. Serranti (Eds.), *CHoPS-05 CD Proceedings*, Tel Aviv, pp. 1–10. ORTRA.

Luding, S. (2008a). Cohesive frictional powders: Contact models for tension. *Granular Matter 10*, in press. accepted.

Luding, S. (2008b). The effect of friction on wide shear bands. *Part. Syst.*. in press.

Luding, S., M. Lätzel, and H. J. Herrmann (2001). From discrete element simulations towards a continuum description of particulate solids. In A. Levy and H. Kalman (Eds.), *Handbook of Conveying and Handling of Particulate Solids*, Amsterdam, The Netherlands, pp. 39–44. Elsevier.

MiDi, G. (2004). On dense granular flows. *Eur. Phys. J. E 14*, 341–365.

Vermeer, P. A., S. Diebels, W. Ehlers, H. J. Herrmann, S. Luding, and E. Ramm (Eds.) (2001). *Continuous and Discontinuous Modelling of Cohesive Frictional Materials*, Berlin. Springer. Lecture Notes in Physics 568.

6 Author

Prof. Dr. rer. nat. Stefan Luding
Particle Technology, Nanostructured Materials, DelftChemTech
TU Delft
Julianalaan 136
2628 BL Delft, Netherlands
Mult Scale Mechanics, CTW, UTwente
POBox 217
7500 AE Enschede, Netherlands
e-mail: `s.luding@utwente.nl`